Biogeosciences Discuss., 8, 11725–11765, 2011
www.biogeosciences-discuss.net/8/11725/2011/
doi:10.5194/bgd-8-11725-2011

Biogeosciences Discussions

Remote sensing of coccolithophore blooms in selected oceanic regions using the PhytoDOAS method applied to hyper-spectral satellite data

A. Sadeghi[1], **T. Dinter**[1,2], **M. Vountas**[1], **B. Taylor**[2], **M. Altenburg-Soppa**[2], and **A. Bracher**[1,2]

[1]Institute of Environmental Physics, University of Bremen, Bremen, Germany
[2]Alfred-Wegener-Institute for Polar and Marine Research, Bremerhaven, Germany

Received: 30 September 2011 – Accepted: 16 November 2011
– Published: 8 December 2011

Correspondence to: A. Sadeghi (sadeghi@iup.physik.uni-bremen.de)

Published by Copernicus Publications on behalf of the European Geosciences Union.

Abstract

In this study temporal variations of coccolithophore blooms are investigated using satellite data. Eight years, from 2003 to 2010, of data of SCIAMACHY, a hyper-spectral satellite sensor on-board ENVISAT, were processed by the PhytoDOAS method to monitor the biomass of coccolithophores in three selected regions. These regions are characterized by frequent occurrence of large coccolithophore blooms. The retrieval results, shown as monthly mean time-series, were compared to related satellite products, including the total surface phytoplankton, i.e., total chlorophyll-*a* (from GlobColour merged data) and the particulate inorganic carbon (from MODIS-Aqua). The inter-annual variations of the phytoplankton bloom cycles and their maximum monthly mean values have been compared in the three selected regions to the variations of the geophysical parameters: sea-surface temperature (SST), mixed-layer depth (MLD) and surface wind speed, which are known to affect phytoplankton dynamics. For each region the anomalies and linear trends of the monitored parameters over the period of this study have been computed. The patterns of total phytoplankton biomass and specific dynamics of coccolithophores chlorophyll-*a* in the selected regions are discussed in relation to other studies. The PhytoDOAS results are consistent with the two other ocean color products and support the reported dependencies of coccolithophore biomass' dynamics to the compared geophysical variables. This suggests, that PhytoDOAS is a valid method for retrieving coccolithophore biomass and for monitoring its bloom developments in the global oceans. Future applications of time-series studies using the PhytoDOAS data set are proposed, also using the new upcoming generations of hyper-spectral satellite sensors with improved spatial resolution.

BGD

8, 11725–11765, 2011

1 Introduction

1.1 Importance of coccolithophores

Phytoplankton play crucial roles in the marine food-web and in the global carbon cycle. Sensitive responses of phytoplankton to the environmental and ecological impacts make them reliable indicators of the variations in climate factors. Coccolithophores (*coccos*) are an abundant taxonomic group of phytoplankton with a wide range of effects on the oceanic biogeochemical cycles (Rost and Riebesell, 2004) and a significant influence on the optical features of surface water (Tyrrell et al., 1999). *Coccos* also affect the atmosphere and climate by emitting dimethylsulfide (DMS) into the atmosphere (Tyrrell and Merico, 2004; Andreae, 1990), where it is converted to the sulfur aerosols and cloud condensation nuclei (CCN) and influence the climate and the Earth's energy budget (Charlson et al., 1987; Andreae, 1990). Among different phytoplankton blooms, *coccos* blooms are very important due to their wide coverage and frequent occurrence (Holligan et al., 1983), as well as their unique biooptical and biogeochemical properties (Brown and Podesta, 1997; Balch, 2004). *Coccos* are the main planktonic calcifiers in the ocean characterized by building up calcium carbonate ($CaCO_3$) plates, called *coccoliths* (Westbroek et al., 1985). Through building and releasing *coccoliths*, *coccos* make a major contribution to the total content of Particulate Inorganic Carbon (PIC or suspended $CaCO_3$) in the open oceans (Milliman, 1993; Ackleson et al., 1994). PIC represents about 1/4 of all marine sediments (Broecker and Peng, 1982) and is regarded as a major oceanic sink for atmospheric CO_2 and by this interacting with the rate of ocean acidification (Balch and Utgoff, 2009). In the same context, increased oceanic CO_2, which is a response to the increase in atmospheric CO_2 (anthropogenic contribution), affects the rate of calcification by *coccos* by reducing the supersaturation state of the carbonate ion (Riebesell et al., 2000). Moreover, sinking through the water column and getting deposited in the sediment (either directly as *coccoliths* and detritus or after being converted into PIC), *coccos* are considered to be one of the main drivers of the biological carbon pump (Raven and Falkowski, 1999;

BGD
8, 11725–11765, 2011

Rost and Riebesell, 2004; Thierstein and Young, 2004) and hence a key component of the global carbon cycle (Westbroek et al., 1993). *Coccos* are known for frequently forming large scale blooms (Holligan et al., 1983), where due to their *coccoliths*, they cause two important optical effects: a very high reflectance from the ocean surface, and a wide impact on the light field in upper ocean (Ackleson et al., 1988; Balch et al., 1989). The most dominant species within the *coccos* taxonomic group is *Emiliania huxleyi* (*E. huxleyi*). *E. huxleyi* is known to be a significant producer of DMS (Keller et al., 1989b; Malin et al., 1992), which affects the planetary albedo (Charlson et al., 1987). *Coccos* blooms succeed diatom blooms in response to increasing stabilization and nutrient depletion of surface waters (Margalef, 1978; Holligan et al., 1983; Lochte et al., 1993). Hence, monitoring *coccos* blooms can also improve our understanding on the global distribution of diatoms. Some former studies aimed to exploit and develop remote sensing methods for monitoring the distribution of *coccos* on a global scale (Groom and Holligan, 1987; Brown and Yoder, 1994a; Brown, 1995; Gordon et al., 2001), as well as studying corresponding blooms on regional scales (Balch et al., 1991; Holligan et al., 1993; Brown and Yoder, 1994b; Brown and Podesta, 1997; Smyth, 2004; Morozov et al., 2010).

1.2 Background of the retrieval method

Coccolithophores frequently form large blooms, which can be visually detected by satellite imageries. Surveying the distribution and development of marine phytoplankton on a global scale (Yoder et al., 1993; Sathyendranath et al., 2004; Alvain et al., 2005) has conventionally been done by retrieving aquatic chlorophyll-*a* concentrations (chl-*a*), as an indicator of phytoplankton biomass (Falkowski et al., 1998). For ocean color remote sensing, several biooptical empirical algorithms (e.g., OC4v4 by O' Reilly et al., 1998) and semi-analytical algorithms (Carder et al., 2004) have been developed, relying on water-leaving radiance detected by satellite sensors at two to five specific wavelength bands. However, due to the phytoplankton biodiversity and differences in the optical properties of phytoplankton groups, remote identification of

BGD
8, 11725–11765, 2011

different phytoplankton functional types (PFTs; see summary by Nair et al., 2008) with improved algorithms and new retrieval methods has recently been in the focus of research (Ackleson et al., 1994; Brown and Yoder, 1994a; Tyrrell et al., 1999; Gordon et al., 2001; Subramaniam et al., 2002; Sathyendranath et al., 2004; Alvain et al., 2005). The development of PFT-based retrieval methods will also improve the estimates of the total phytoplankton biomass and deepen the understanding of the oceanic biogeochemical cycles. Based on this demand, the PhytoDOAS method was established to discriminate major phytoplankton groups based on their specific absorption footprints on the backscattered radiation from the ocean (Bracher et al., 2009).

PhytoDOAS is an extension of Differential Optical Absorption Spectroscopy, DOAS (Perner and Platt, 1979; Platt, 1994) into the aquatic medium. By applying the PhytoDOAS method to hyper-spectral satellite data, provided by the SCIAMACHY sensor (on-board ENVISAT), the global distributions of two main phytoplankton groups, diatoms and cyanobacteria, have been derived. By improving the method through *multi-target fitting*, two more PFTs, *coccos* and dinoflagellates have been distinguished recently (Sadeghi et al., 2011). To test this improvement, SCIAMACHY data from 2005 have been globally processed using the improved PhytoDOAS method. The successful retrieval of *coccos* was proven by comparisons with the global distribution of PIC, provided by MODIS-Aqua level-3 products and comparison with the *coccos* modeled data obtained from NASA Ocean Biochemical Model, NOBM (Gregg et al., 2003; Gregg and Casey, 2007). In addition, two sample *coccos* blooms, detected by satellite imagery, were identified by applying the improved PhytoDOAS to the SCIAMCHY data: one located around New Zealand, reported in December 2009 as a RGB image by MODIS (Sadeghi et al., 2011); and the other one in the North Atlantic in August 2004.

1.3 Objectives

The main interest of this study was to apply the PhytoDOAS method for quantitative remote sensing of *coccos* using satellite data. Due to the crucial role of *coccos* in the global biogeochemical cycles, this satellite-based method can be used for monitoring

BGD
8, 11725–11765, 2011

temporal and spatial variations of *coccos* on a global scale, which in turn can be used (as a phenomenal study of phytoplankton dynamics) for studying the impacts of a varying climate on marine phytoplankton (Winder and Cloernet, 2010). To show this capacity, *coccos* blooms in selected regions were monitored over eight years and their inter-annual variations were investigated along with the temporal variations of certain geophysical parameters. On the other hand, PhytoDOAS takes the following factors into account, which are often not considered in current biooptical methods based on band-ratio algorithms: the phytoplankton absorption spectra, the existence of multiple PFTs and the light penetration depth in the water. Therefore, the above specific capacities of the method are investigated by this study. More specifically, concerning *coccos* retrieval, while other phytoplankton pigments cause a decrease in backscatter radiance mostly in the blue part (and slightly in the green), *coccos*, due to their calcite plates, affect the solar irradiance uniformly in both the blue and the green (Gordon et al., 1988). Furthermore, as *coccos* blooms cause flattening of the reflectance spectrum, the standard ratio pigment algorithms (Gordon and Morel, 1983) will not provide correct pigment retrievals within the blooms (Balch et al., 1989; Balch, 2004); while, by retrieving the differential absorption features, the PhytoDOAS method has the potential to obtain results on PFT chl-*a* in high *coccos* regions, when hyper-spectral variations are still visible. In this sense, retrieving *coccos* blooms provides a reliable application to test the improved PhytoDOAS method.

2 Study setup

2.1 Initial tests and selection of regions

Regarding the fact that the whole *coccos* group can not be observed through in-situ measurements, the direct comparison of the retrieved *coccos* with the in-situ data is too difficult. More precisely, with analyzing water samples by microscopy or with the Continuous Plankton Recorder (CPR) only the larger cells (> 5 and > 10 µm, respectively) can

BGD
8, 11725–11765, 2011

be identified. From HPLC and flow-cytometric analysis only the groups of haptophytes or nano-eukaryotes, respectively (to both coccolithophores belong to), can be identified. In addition, there is a significant difficulty associated with the collocation of the in-situ point measurements to the large SCIAMACHY ground pixels of 30 km by 60 km. Therefore, so far, the PhytoDOAS *coccos* results, instead of validation, were compared to the global distribution of PIC obtained from the MODIS-Aqua level-3 products (this was after the preliminary comparisons with the NOBM *coccos* modeled data). The reason behind is, since the concentration PIC is proportional to the suspended *coccoliths* in surface waters, it is regarded as the main indicator of *coccos* Balch et al. (2005). Very good agreements were observed in patterns of *coccos* and PIC on a monthly and seasonal basis (Sadeghi et al., 2011). Moreover, *coccos* chl-*a* results were compared to the total chl-*a* (provided by GlobColour merged data), as the maximum limit of observed chl-*a* for *coccos*. Figure 1 illustrates a sample comparison of these three products for August 2005, showing consistent patterns between *coccos* (upper panel) and PIC (middle panel), followed by partially similar patterns of the total chl-*a* (lower panel).

To monitor the development of *coccos* blooms, regions of high occurrence were selected based on the following procedure: first, a global distribution of *coccos*, mapped by Brown and Yoder (1994a) and Brown (1995) was considered; secondly, eight years of global distribution of PIC, from MODIS-Aqua level-3 monthly products was monitored; and finally *coccos* field studies were analyzed (Brown and Podesta, 1997; Balch et al., 1991; Holligan et al., 1993; Garcia et al., 2011; Raitsos et al., 2006; Painter et al., 2010; Burns, 1977; Tilburg et al., 2002). Based on these pre-investigations, three regions have been selected (Fig. 2), located in the North Atlantic (south of Iceland), the South-West Atlantic (north of the Falkland Islands), and the South-West Pacific (southwest of New Zealand, surrounded by the Tasman Sea). For simplicity the regions were labeled as: *nAtl*, *sAtl* and *sPac*, respectively. The regions were been selected to be $10^{\circ} \times 10^{\circ}$ areas, which regarding their latitudinal distributions means almost the same area for *sAtl* and *sPac* and smaller for *nAtl*. As shown in Fig. 2 on a background of the

BGD
8, 11725–11765, 2011

MODIS-Aqua PIC product, two regions (*sAtl* and *sPac*) are located in the *Great Calcite Belt* (Balch et al., 2011), which is a great latitudinal belt of elevated PIC concentrations, containing over one-third of all global PIC. The *Great Calcite Belt* is located all the way around the Southern Ocean near the sub-Antarctic front and polar front (between about 30° S and 60° S). To retrieve *coccos* dynamics in selected regions, the PhytoDOAS method according to Sadeghi et al. (2011) was applied to SCIAMACHY data (from January 2003 to December 2010) for each region. Absorption spectrum of *Emiliania huxleyi* (*E. huxleyi*) was used for the *coccos* target, because *E. huxleyi* is generally the dominant species in this group. The principles of this improved PhytoDOAS method as well as all needed reference spectra, were explained in details in Bracher et al. (2009); Sadeghi et al. (2011).

2.2 Satellite and modeled data

Satellite data used for the PhytoDOAS method must be spectrally highly resolved. This requirement is met using the data collected by SCIAMACHY (SCanning Imaging Absorption spectroMeter for Atmospheric CHartographY), a sensor on-board ENVISAT (ENVIronmental SATellite of European Space Agency, ESA) launched in 2002. This sensor covers a wide wavelength range (from 240 to 2380 nm in 8 channels) with a relatively high spectral resolution, ranged from 0.2 to 1.5 nm (Bovensmann et al., 1999). In this study, nadir-viewing SCIAMACHY data in specific wavelength ranges of UV and visible were used, for which the spectral resolution is ranging from 0.24 to 0.48 nm. These data, used to built up the measured *optical-depth*, include backscattered radiation from oceanic surfaces (case-I waters), with a spatial resolution of about $30 \times 60\,km^2$, and solar radiation measured at the top of the atmosphere in the same wavelength range. Within PhytoDOAS, SCIAMACHY data were exploited at two wavelength ranges: First, the absorption spectra of the target PFTs were fitted using the visible data within the fit-window of 429 to 521 nm; secondly, part of SCIAMACHY UV data (from 340 to 385 nm) was used to estimate the *light-penetration depth* through retrieving the spectral signature of vibrational Raman scattering of water molecules (Vountas

BGD
8, 11725–11765, 2011

et al., 2003, 2007). To compare and evaluate the *coccos* retrieval results and to investigate their probable correlations with climate factors, four other satellite products were collected for the selected regions from January 2003 to December 2010 as follows: (1) total chl-*a* from ESA's ocean-color dataset, GlobColour, providing merged data from three major ocean-color sensors: MODIS-Aqua, MERIS and SeaWiFS, with 4 km grid resolution (for details see: http://www.globcolour.info); (2) PIC data from MODIS-Aqua level-3 products with 9 km grid resolution (see details on MODIS web-page: http://modis.gsfc.nasa.gov); (3) sea surface temperature (SST) from Advanced Very High Resolution Radiometer sensor (AVHRR: http://nsidc.org/data/avhrr) with a 4 km spatial resolution (from Pathfinder V5); and finally (4) surface wind-speed data derived from the Advanced Microwave Scanning Radiometer-Earth Observing System (AMSR-E) sensor, globally gridded at $0.25^{\circ} \times 0.25^{\circ}$ (more information at http://remss.com).

The MLD data were obtained from Ocean Productivity (http://orca.science.oregonstate.edu/1080.by.2160.monthly.hdf.mld.fnmoc.php). For this data product, the MLD monthly data (after June 2005) are provided based on the MLD output of FNMOC (Fleet Numerical Meteorology and Oceanography Center). FNMOC's MLD is determined through the TOPS (Thermal Ocean Prediction) model by identifying the depth where the temperature is 0.5 degree lower than the value at the surface (the so-called isothermal layer depth, ILD). In general, apart from the high latitudes (above $\pm 70^{\circ}$), the IDL is a good approximation of MLD. For the period before July 2005, the MLD data were obtained from the Ocean Productivity merged data set from the SODA (simple ocean data assimilation) model. The grid resolution of the MLD monthly data is 1/6 degree.

2.3 Further processing of the results

The data of the different parameters were represented as time series of monthly mean values within the same time period. PhytoDOAS results for all pixels within the selected regions were averaged for each month; MODIS-Aqua PIC data, AVHRR SST data and AMSR-E wind-speed data were directly collected as monthly-mean values; daily

BGD
8, 11725–11765, 2011

products of GlobColour total chl-*a* was converted into monthly mean values. Then, for each region, the time-series of all six parameters were built up from January 2003 to December 2010. In the post-processing of the PhytoDOAS retrieved data, two criteria for removing data-points of poor quality were applied: to filter out pixels with poor fit quality, only fit results with *Chi-Square*, χ^2, values below 0.001 were used and a threshold of pixel numbers was applied to the monthly-mean to remove data points that were averaged over an insufficient number of remaining pixels (within a month). The minimum number of pixels (per month) for considering a monthly mean as an acceptable point, was determined by building an occurrence histogram, with the number of pixels per month as the random variable. Taking a coverage less than 10 % of total occurrences as the lower limit, the threshold value was ranging, depending on the region, from 40 to 90 minimum observations per month.

It should be noted that, while ocean colour observations in general cover only the surface waters, the PhytoDOAS retrieval results are the average value over the light path observed by the satellite. However, the signal measured by the satellite is not weighted equally by the different depths and the surface concentration are dominating the determined values. Therefore, one has to keep in mind that our study is focusing only on the surface waters' phytoplankton phenology.

3 Results and discussion

3.1 Time series of biological and geophysical parameters

The time series from January 2003 to December 2010 of all parameters over the three selected regions *nAtl*, *sAtl* and *sPac* are shown in Figs. 3–5, respectively. These time-series comprise monthly mean values of the following parameters: (a) *coccos* chl-*a* (denoted by *Ehux*) retrieved by PhytoDOAS, (b) GlobColour total chl-*a*, (c) PIC concentration from MODIS-Aqua, (d) MLD estimates provided by Ocean Productivity, (e) SST from AVHRR dataset, and (f) surface wind-speed from AMSR-E dataset. In

BGD
8, 11725–11765, 2011

the time-series of the PhytoDOAS *coccos* are some missing points, due to the post-processing of the retrieved data; i.e., the fit-quality filter (χ^2) and the average-quality condition (number of pixels per month).

Due to these gaps the *coccos* time-series, compared to the time-series of the other parameters, depict more artifact features, which must be distinguished from their natural irregularities. The main reason for this anomaly is that SCIAMACHY (primarily designed for atmospheric missions), compared to usual ocean color sensors, e.g., MODIS-Aqua, SeaWiFS and MERIS, has a very coarse spatial resolution. The characteristic of having large ground pixels makes its surface UV-visible data very sensitive to cloud contaminations, as compared to other sensors with high spatial resolutions. Therefore, the time-series of PIC, provided by MODIS-Aqua, and the time-series of total chl-*a*, obtained from GlobColour merged data, show very few gaps. However, there are still enough data points in the *coccos* time-series, for comparing *coccos* temporal variations with the other parameters.

In the time-series of the *nAtl* region (Fig. 3) all parameters show a clear annual cycle; however, for some of the parameters (not for SST and MLD) the inter-annual cyclical periods of high intensities are deviating from one year to another; e.g., from 2008 to 2009 for *coccos* and PIC the period between the maxima is reduced to 10 months, while it is 11–14 for all other years (e.g. 2007 to 2008). However, for GlobColour total chl-*a* the intervals between successive maxima for the periods 2008/2009 and 2007/2008 are about 13 and 10 months, respectively. It can also be seen that the timing of the maximum conc. of *coccos*, PIC and total chl-*a* are positively correlated. These maxima are negatively correlated with the MLD, as they should be, because the rate of *coccos* growth increases rapidly with shoaling of MLD (Raitsos et al., 2006). More precisely, all three phytoplankton-based time-series in Fig. 3 imply that the phytoplankton prosperity is associated with a rapidly decreasing MLD, and reaches its maximum when MLD begins its period of constant minimum. The North Atlantic is generally characterized by an extremely deep winter mixed layer, which causes very low phytoplankton activity in wintertime, which can be seen as well in Fig. 3. The

BGD
8, 11725–11765, 2011

phytoplankton and PIC maxima coincide with the high positive gradient of SST, i.e, SST peaks always appear delayed to the phytoplankton peaks, which is in accordance with the results of Raitsos et al. (2006). Theoretically, it is expected that the maxima of the three phytoplankton-based time-series follow in a sequence as the time elapses: total chl-*a* followed by *coccos* and finally PIC, as *coccos* start growing when the necessary nutrients for the growth or the survival of other species are scarce (Margalef, 1978; Holligan et al., 1983). On the other hand, the PIC concentration is expected to be proportional to the amount of *coccoliths*, which can be either attached to the living *coccos* or detached from them and suspended in the water, even after the disappearance of the *coccos*. However, this sequence could not be reproduced in our time-series, except for the year 2008. In fact, the peaks of total chl-*a* and PIC appear more or less at the same time, while *coccos* peaks often follow the two former peaks with a slight delay. This systematic behavior might be originated from the large monthly time interval used for averaging the retrieved products and setting up the *coccos* time-series (the lower subplots in Figs. 3–5); one-month period is probably larger than the real, rather weekly, temporal rhythm of phytoplankton dynamics.

While the SST, the MLD, and also the PIC conc. show clear annual cycles in the regions of *sAtl* and *sPac* (Figs. 4 and 5), the annual patterns for *coccos* and total phytoplankton chl-*a* are much more irregular than in the *nAtl*. This can be explained by the very dynamic wind-speed patterns observed in *sAtl* and *sPac*. As surface wind-stress forces the vertical motion in the water column (in addition to the horizontal motions as surface waves), it is affecting the stratification and the nutrient regime. As the *coccos* are only a group of the phytoplankton it is expected that total chl-*a* would vary more smoothly than this specific PFT. Moreover, there are several other possible reasons for the irregular phytoplankton and PIC conc. in the *sAtl* region:

– The general circulation in the *sAtl* is influenced by the collision of two main currents: the Malvinas (Falklands) current, transporting northwards sub-Antarctic cold and fresh waters and the Brazil current, carrying southwards subtropical saline and warm waters (Gordon, 1989; Spadone and Provost, 2009). The

BGD
8, 11725–11765, 2011

Brazil/Falklands confluence is an energetic and complex region of interaction and mixing of water masses (Brandini et al., 2000; Oliveira et al., 2009).

- The *sAtl* is located at the eastern part of the Patagonian shelf, which is regarded as one of the richest areas of primary production (Bianchi et al., 2005, 2009; Schloss et al., 2007), and features recurring large *coccos* blooms (Longhurst, 1995; Painter et al., 2010). The Patagonian shelf, between 38° S and 51° S, is located southwest of the confluence zone and therefore is affected by that. Apart from that, according to hydrography observations and satellite imagery (Saraceno et al., 2004; Bianchi et al., 2005; Romero et al., 2006), there are two other factors affecting the hydrography of the Patagonian shelf: the *shelf break front*, which is a transition between the Malvinas current and shelf waters, existing in both winter and summer seasons (being stronger in the summer months) and the energetic *tidal fronts*, with pronounced seasonal variability, causing the vertical stratification of water masses (Sabatini et al., 2004; Bianchi et al., 2005).

- The non-cyclic aerosol-load and dust transport from the Patagonian desert into the South Atlantic Ocean (atmospheric and riverine), affecting the phytoplankton productivity of the Patagonian shelf by changing the nutrient regime (Erickson et al., 2003).

- The South-Atlantic Anomaly (SAA) of the Earth's magnetic field affects most of satellite measurements over parts of South-America and South-Atlantic. Although the SAA region lies roughly between latitudes 5° S and 40° S, its precise shape, size and strength varies with the seasons (http://sacs.aeronomie.be/info/saa.php). Hence, our *sAtl* region, residing between 40° S and 50° S, could be partly affected by SAA.

The high variations and anomalies seen in the *sPac* time-series, can be attributed to its location, which is surrounded by the Tasman Sea. The Tasman Sea is one of the fastest warming areas in the Southern Hemisphere ocean (Neuheimer et al., 2011;

BGD
8, 11725–11765, 2011

Ridgway, 2007), because of both, globally rising SST and specific local effects, such as the characteristic of the warm poleward waters of the East Australian Current (EAC) (Cai et al., 2005; Ridgway, 2007). Moreover, large eddies occurring in the Tasman Sea have a great contribution to the vertical mixing within the upper ocean. This increased mixing effectively counteracts the winter stratification and results in a varying chl-*a* seasonal cycle (Tilburg et al., 2002). In this sense, the seasonal cycle of chl-*a* in *sPac* should be pronounced, similar to the North Atlantic, which has very strong mixing. Whereas the seasonality in the time-series of GlobColour total chl-*a* for *sPac* is rather weak (less pronounced than in *coccos*). This observation suggests a demand for a regional improvement of the chl-*a* algorithms from ocean-color sensors, at least for the South-West Pacific.

In *sPac*, higher chl-*a* for *coccos* than for the total phytoplankton is observed. Further investigations showed why the PhytoDOAS *coccos* method is overestimating the coccolithophore chl-*a* (Fig. 5): studies by Burns (1977) and Rhodes et al. (1995) showed that in the Tasman Sea and also around New Zealand (i.e., in *sPac*) the dominant *coccos* species is varying between *E. huxleyi* and *Gephyrocapsa oceanica* (*G. oceanica*). Whereas, in this study the PhytoDOAS retrieval of *coccos* was based on the specific absorption spectrum of *E. huxleyi*. Figure 6 illustrates the specific absorption spectra of these two *coccos* species, *G. oceanica* and *E. huxleyi*, which were measured on cultures obtained from the isolation of these species from natural samples in different regions. As illustrated in Fig. 6, the specific absorption values of *G. oceanica* are much lower than the values of *E. huxleyi*. The reason is that the former species has, compared to *E. huxleyi*, much more chl-*a* pigment contents per cell. Hence, retrieving *G. oceanica* from a *E. huxleyi* specific absorption spectrum results in an overestimation of chl-*a* content. However, the similar absorption patterns of these two species ensures that the retrieval process can identify them as *coccos* target. All together, these samples show the spatial variations in phytoplankton absorption within the same phytoplankton group. This feature and the different photo-acclimation, also changing the specific phytoplankton absorption, can affect the result of the PhytoDOAS retrieval.

BGD
8, 11725–11765, 2011

The ratios of the GlobColour total chl-*a* to the PhytoDOAS retrieved chl-*a* of *coccos* are depicted in Fig. 7 for the three study regions: The retrieved chl-*a* of *coccos* seem to be overestimated (which is associated with values less than one) in many months. Especially pronounced is this feature in the *sPac* region (lower panel). The reasons of the relatively higher coccos for this region have already been discussed above. However, in *nAtl* and *sAtl* (upper and middle panels in Fig. 7, respectively), there are alternating patterns in the months, when the *coccos* chl-*a* exceed the GlobColour total chl-*a*. In both regions the *coccos* chl-*a* exceed the total chl-*a* mostly after the summer bloom, i.e., after June in *nAtl* and for the austral summer in *sAtl* (except for the year 2010). Considering that these regions are characterized as high activity areas of *coccos* blooms (Holligan et al., 1993; Raitsos et al., 2006; Painter et al., 2010; Garcia et al., 2011), along with the fact that the large reflectance from coccolithophore-rich surface waters affect the performance of the standard chl-*a* algorithms (Gordon et al., 1988; Ackleson et al., 1988; Balch et al., 1989; Balch, 2004), the overestimation of *coccos* observed in Fig. 7 may be assigned to a proposed underestimation of chl-*a* during the *coccos* blooms for the GlobColour data set. This algorithm is based on reflectance ratios. The final validation of the *coccos* chl-*a* will be part of a future study by comparison of the PhytoDOAS data product to a combination of the above mentioned in-situ measurements of coccolithophores.

3.2 Interconnections between biological and geophysical parameters

To investigate the driving factors behind the development and degradation of *coccos* biomass, the correlation coefficients between PhytoDOAS *coccos* chl-*a* and all other parameters were computed (Fig. 8, left panels). Similarly, the correlation coefficients between PIC conc. and the other parameters were determined (Fig. 8, right panels).

In *nAtl* the retrieved *coccos* correlated positively with the total chl-*a*, PIC and SST, and negatively with MLD and surface wind-speed (upper left panel in Fig. 8). These results are in accordance with the reported dependence of *coccos* on raising SST (or high surface irradiances), shallow MLD (or shallow stratification) and non-turbulent

BGD
8, 11725–11765, 2011

waters (Tyrrell and Taylor, 1996; Nanninga and Tyrrell, 1996; Raitsos et al., 2006), respectively. The correlation pattern of PIC conc. (Fig. 8 upper-right panel) was very similar to the PhytoDOAS *coccos*, with close values of correlation coefficients (except being higher correlated to the GlobColour total chl-*a* and being more inversely correlated to MLD). This similarity indicates the good agreement between the PhytoDOAS *coccos* and the MODIS-Aqua PIC in *nAtl*.

However, in *sAtl* the retrieved *coccos* were hardly correlated with total chl-*a* and PIC (Fig. 8, middle-left panel); possible reasons have been discussed before (Sect. 3.1). The correlations of *coccos* with the geophysical parameters were weaker, compared to *nAtl*, but showing the same pattern. Moreover, despite the anomaly sources mentioned for this region, the correlation of *coccos* with SST, was similar to the situation in *nAtl*, which indicates again the vital importance of the rising SST (or high solar radiation) for occurring *coccos* blooms. The correlations of PIC with other parameters in *sAtl* (middle-right panel) showed the same pattern and levels as in *nAtl*, but weaker with surface-wind, which can be assigned to the complicated regimes of surface currents in this region as explained before.

In *sPac* (Fig. 8, lower-left panel) the correlations between *coccos* and total chl-*a* and PIC slightly better than in *sAtl*, but there were less dependence on SST and MLD. The latter feature can be assigned to the dynamic surface-wind patterns observed in this region, which is associated with the presence of large eddies in the Tasman Sea. These eddies, originated from the separation of the EAC, migrate southwards into the Tasman Sea and cause regions of intense upwelling and downwelling (Tilburg et al., 2002), which results in turn in a strong seasonal cycle of phytoplankton activity with the associated anomalies. Moreover, the specific floor topography of the Tasman Sea, i.e., the presence of an important mid-ocean ridge (van der Linden, 1969), and its effects on the surface currents and vertical motions of the water bodies should be kept in mind.

The highest correlation observed between PIC conc. and GlobColour totalchl-*a*. This is not surprising as the algorithms of these two products use the reflectance information from the same wavelength-bands and both products are obtained from the

BGD
8, 11725–11765, 2011

high spatially resolved satellite data (in contrast to the coarse spatially resolved SCIAMACHY data). Moreover, MODIS-Aqua itself is one of the three ocean color sensors used by GlobColour project to provide the merged data (the other two sensors are SeaWiFS and MERIS).

Since it is thought that the blooms of *coccos* usually follow diatom blooms, the time series of diatoms and *coccos* biomass in the selected study regions is shown in Fig. 9. As mentioned above, in the PhytoDOAS multi-target fit, *coccos* are simultaneously retrieved with diatoms and dinoflagellates. In all three regions chl-*a* of diatoms was always higher than *coccos*, as is expected in general (Goldman, 1993; Clark et al., 2002). However, the patterns of the temporal variations of diatoms do not vary significantly from the counterpart patterns of *coccos*. This can be again assigned to the large time period for averaging the PhytoDOAS data, which is much longer than real time-frame of phytoplankton blooms. Due to this averaging, maxima of monthly *coccos* or diatoms' chl-*a* were probably smaller than the absolute maxima they reach during the blooms.

3.3 Annual pattern of phytoplankton development associated with the developments of geophysical variables in selected regions

Figure 10 illustrates the linear trends of five parameters for eight years of data (from 2003 to 2010) for the three study regions. To reduce the effects of seasonality on the trend results, and to focus on the inter-annual variations of the parameters in phytoplankton prosperity seasons, only the months that cover the regional spring and summer were taken into account. Additionally, the ocean color winter time data only contain very few ground pixels per month which also increases the uncertainty to the monthly mean values. Hence, for *nAtl* six months from April to September, and for *sAtl* and *sPac* seven months from September to March were considered. Linear regressions were computed for the monthly mean data (Fig. 10 upper panel) and for the anomaly time-series data (Fig. 10 lower panel); here each data-point was obtained by subtracting the initial monthly mean (e.g., June 2004) from the climatological mean of that

BGD
8, 11725–11765, 2011

particular month (i.e., mean value of all June months over eight years). We refer hereafter to these approaches as *simple trend* and *anomaly trend*, respectively. No linear trends for MLD are shown in Fig. 10, because the MLD data, as modeled data, involve far more approximations than in the satellite-based retrieved products, making the comparison not suitable; moreover, the order of magnitudes of the MLD trends are higher than the linear trends of the retrieved products, which could cause illustration problem. Following table contains the MLD linear trends in three regions, which were calculated by both *simple trend* and *anomaly trend* approaches.

Considering the *simple trend* values (Fig. 10 left panel), *coccos* grew negligibly in *nAtl* and chl-*a* decreased in the two southern regions by different rates; total chl-*a* increased in all regions, PIC decreased strongly in *nAtl* and *sAtl*, while it strongly increased in *sPac*. This may be caused by the strong SST-rise in the Tasman Sea (Tilburg et al., 2002), even though this SST rise was not observed in our *sPac* simple trend; however, the decreasing rate of SST in *sAtl* and *sPac* was clearly followed by the decrease of *coccos* and consistently, the rate of increase of SST in *nAtl* was associated, at a small rate, with the increase of *coccos*; the surface wind-speeds decreased in *nAtl* and *sPac*, while they slightly increasing in *sAtl* . Only in *nAtl* was the decreasing rate of wind-speed associated with an increasing rate of *coccos*. Considering that there is also no constant relationship between rates of change of wind-speed and PIC in the three regions, it can be inferred that in the studied time-scale of about one decade, the rate of change of *coccos* was not determined by the rate of wind-speed. Comparing the values of the *simple trend* with the *anomaly trend* values (Fig. 10 left panel), both showed similar results. Only the SST anomaly trends were different, especially in *sAtl* and *sPac* where the trends were even reversed. To summarize, the results were comparable and the anomaly trend was more appropriate because it removed the seasonal effect.

BGD
8, 11725–11765, 2011

3.4 Climatology analysis

Figure 11 illustrates the climatology curves for the corresponding six parameters in the three selected regions. Each data-point here depicts the mean value of a certain month over eight years' data of the respective time series. In nAtl, the *coccos* reached their maximum in August, whereas in *sAtl* and *sPac* two maxima were reached annually, a smaller one in austral spring (between September and October) and a higher one in austral summer (between February and March). The occurrences of two *coccos* blooms annually in the Southern Hemisphere has been reported before (Balch et al., 2011). In *sPac* these maxima were not as pronounced, showing another weak maximum in May. This may be caused by the effect of large eddies existing in the Tasman Sea. However, the *coccos* maximum in austral spring in *sPac* was also observed by studying SeaWiFS data (Tilburg et al., 2002).

The GlobColour total chl-*a* showed an annual peak spreading over spring and summer, with two weak shoulders in *nAtl* (higher in June and a smaller in August), one wide peak in *sAtl* from October to January and only a minor peak in *sPac* from October to February. These results in *nAtl* and *sAtl* suggest that the *coccos* are the dominant phytoplankton group succeeding the main bloom in late summer, which again supports the argument that *coccos* are favored when nutrients are depleted. However, the almost flat curve of GlobColour total chl-*a* in *sPac* is not consistent with SeaWiFS results presented in Tilburg et al. (2002) for the Tasman Sea. MODIS-Aqua PIC showed five months (May to September) of enhanced conc. in *nAtl* with two pronounced shoulders in June and August, coinciding temporally with the maxima of GlobColour total chl-*a*, while only the latter peak was coinciding with the *coccos* annual maximum. This may indicate that either during the first total chl-*a* peak (in June) *coccos* were contributing significantly to the biomass and the PhytoDOAS algorithm is underestimating the *coccos* chl-*a*, or the PIC algorithm is partly incorrect in this region. The PIC climatology curves in *sAtl* and *sPac* varied quite smoothly (similar to each other), with a peak in December/January, which is more pronounced in *sAtl*. The patterns of PIC climatology

BGD
8, 11725–11765, 2011

in these regions followed the GlobColour total chl-*a* between March and October. The climatology curves of MLD, SST and wind-speed clearly supported the expected geophysical conditions for the formation of *coccos* blooms.

4 Conclusions

We studied the developments of coccolithophore and total phytoplankton blooms and PIC conc. in three selected regions have been studied from January 2003 to December 2010 with satellite data. The time series results of these three phytoplankton-based products reveal the seasonal bloom cycles in a regular order with fairly good accordance to each other. In the *nAtl* region one *coccos* maximum was regularly observed in the summer, while in the *sAtl* and *sPac* regions two maxima in austral spring and summer occurred. The maxima for total chl-*a* and PIC conc. were during the same time period, but in both hemispheric regions only appeared once per year over a longer time period (4–5 months). The results show that the *coccos* blooms generally dominate the total phytoplankton maxima in late summer (August/September in *nAtl* and February/March in two other regions). In the *nAtl* and *sAtl* regions the maximum concentrations are comparable for all three parameters, while they are much lower (70–50 %) in the *sPac* regions. Comparisons to time series of geophysical parameters clearly show that the phytoplankton growth is related to shallow MLDs, low wind-speed, and high and sharp-rising SSTs. Overall, the accordance of the three ocean color data products was better in *nAtl*, as compared to *sAtl* and *sPac*. The major environmental factors affecting the Patagonian shelf and the Tasman Sea have been briefly mentioned, in order to address the possible causes of turbulent and mixing effects in *sAtl* and *sPac*, respectively. The specific regional characteristics in *sAtl* and *sPac*, probably cause effects in smaller time scales than a month. However, our time series study had to be limited to the monthly resolution because of the coarse spatial resolution and limited global coverage of the available hyper-spectral satellite data used for the PhytoDOAS *coccos* retrieval. Applying the PhytoDOAS method to upcoming hyper-spectral satellite

BGD
8, 11725–11765, 2011

sensors, e.g., the Sentinel-5-Precursor (planned to launch in 2014) with $7 \times 7\,km^2$ pixel size and global coverage within two days, will allow the weekly-based monitoring of such phytoplankton blooms dynamics.

The outcome of the study proves that the PhytoDOAS *coccos* data show valuable results, even though there are still sources of uncertainties in the retrieval, to be accounted for, e.g., the spatial variations in the absorption spectra. It should be noted that this product is based on a new method, mostly independent from biological a priori data, as opposed to the standard ocean color products. This retrieval method can be reliably used for remote identification of *coccos* and tracking its bloom developments in the global ocean. For better analysis and interpretation of the results, more investigations on the geophysical parameters ruling the regional climate, as well as on local biological conditions will be done for each region. For instance, due to the importance of light for the formation of *coccos* blooms (Nanninga and Tyrrell, 1996), the variation in solar radiation must be included (e.g., regional time series of water leaving radiance at 555 nm, as referred by Raitsos et al. (2006)). The regional variations of nutrient regime, especially phosphate and nitrate, using appropriate modeled data is the other supplementary work to do. Regional adaptations of the PhytoDOAS *coccos* retrieval are planned in order to account for the spatial variations in specific absorptions with respect to the dominating *coccos* species. In general, to avoid the uncertainties associated with the spatial variations in phytoplankton absorption, an alternative approach would be to establish a multi-regional PhytoDOAS retrieval, using different sets of PFTs' absorption spectra, representing the main regions. For this purpose, the biogeographical provinces presented by Longhurst (1998) could provide a good criterion for dividing the world oceans into the regions. The PhytoDOAS *coccos* data will be validated with available in-situ measurements (e.g., Continuous Plankton Recorder or specific *coccos* cell counts). The data shall also be compared to chl-*a* conc. of haptophytes inferred from HPLC pigment analysis. However, in-situ data also have to be treated with care as they either only consider the large *coccos* via microscopic techniques or, as for the HPLC derived information, also other haptophyte species besides *coccos*; moreover,

BGD
8, 11725–11765, 2011

matching the in-situ point measurements to the large satellite ground pixels is always a challenging task. Time-series studies for other regions of particular interest (e.g., Bering Sea) are planned in order to assess the overall global picture of *coccos* distributions.

Acknowledgements. We are thankful to ESA, DLR, and the SCIAMACHY Quality Working Group (SQWG) for providing us with SCIAMACHY level-1 data. We thank NASA-GSFC for MODIS PIC images and data. We are grateful to NASA and ESA, particularly to the GlobColour project, for processing and supplying satellite total chl-*a* data. We are thankful to AVHRR for providing the SST data, AMSR-E for the surface wind-speed products and also Ocean Productivity for the monthly MLD data. We thank Sebastian Rocitta (AWI) for providing us cultures of Gephyrocapsa and *E. huxleyi*, Sonja Wiegmann (AWI) and Marta Kaspar (AWI) for assistance with the absorption measurements. Funding was provided by the HGF Innovative Network Funds (Phytooptics). Funding for TD was supplied via the EU project SHIVA-226224-FP7-ENV-2008-1. This work is a contribution to the "Earth System Science Research School (ESSReS)", an initiative of the Helmholtz Association of German research centers (HGF) at the Alfred Wegener Institute for Polar and Marine Research. Many thanks to Klaus Grosfeld, the coordinator of ESSReS, for supplementary supports to the first author.

References

Ackleson, S. G., Balch, W. M., and Holligan, P. M.: White waters of the Gulf of Maine, Oceanography, 1, 18–22, 1988. 11728, 11739

Ackleson, S., Balch, W. M., and Holligan, P. M.: Response of water leaving radiance to particulate calcite and chlorophyll-*a* concentrations: A model for Gulf of Maine coccolithophore blooms, J. Geophys. Res., 99, 7483–7499, 1994. 11727, 11729

Alvain, S., Moulin, C., Dandonneau, Y., and Breon, F. M.: Remote sensing of phytoplankton groups in case 1 waters from global SeaWiFS imagery, Deep-Sea Res. Pt. I, 52, 1989–2004, 2005. 11728, 11729

Andreae, M. O.: Ocean-atmosphere interactions in the global biogeochemical sulfur cycle, Mar. Chem., 30, 1–29, 1990. 11727

Balch, W. M.: Re-evaluation of the physiological ecology of coccolithophores, in: Coccol-

BGD

8, 11725–11765, 2011

ithophores. From Molecular Processes to Global Impact, edited by: Thierstein, H. R. and Young, J. R., Springer-Verlag, Berlin, 165–190, 2004. 11727, 11730, 11739

Balch, W. M. and Utgoff, P. E.: Potential interactions among ocean acidification, coccolithophores, and the optical properties of seawater, Oceanography, 22(4), 146–159, 2009. 11727

Balch, W. M., Eppley, R. W., Abbott, M. R., and Reid, F. M. H.: Bias in satellite-derived pigment measurements due to coccolithophores and dinoflagellates, J. Plankton Res., 11, 575–581, 1989. 11728, 11730, 11739

Balch, W. M., Holligan, P. M., Ackleson, S. G., and Voss, K. J.: Biological and optical properties of mesoscale coccolithophore blooms in the Gulf of Maine, Limnol. Oceanogr., 36, 629–643, 1991. 11728, 11731

Balch, W. M., Gordon, H. R., Bowler, B. C., Drapeau, D. T., and Booth, E. S.: Calcium carbonate measurements in the surface global ocean based on moderate-resolution imaging spectroradiometer data, J. Geophys. Res., 110, C07001, doi:10.1029/2004JC002560, 2005. 11731

Balch, W. M., Drapeau, D. T., Bowler, B. C., Lyczskowski, E., Booth, S., and Alley, D.: The contribution of coccolithophores to the optical and inorganic carbon budgets during the Southern Ocean gas exchange experiment: new evidence in support of the Great Calcite Belt hypothesis, J. Geophys. Res., 116, C00F06, doi:10.1029/2011JC006941, 2011. 11732, 11743

Bianchi, A. A., Bianucci, L., Piola, A. R., Pino, D. R., Schloss, I., Poisson, A., and Balestrini, C. F.: Vertical stratification and air-sea CO_2 fluxes in the Patagonian Shelf, J. Geophys. Res., 110, C07003, doi:10.1029/2004JC002488, 2005. 11737

Bianchi, A. A., Pino, D. R., Perlender, H. G. I., Osiroff, A. P., Segur, V., Lutz, V., Clara, M. L., Balestrini, C. F., and Piola, A. R.: Annual balance and seasonal variability of sea-air CO_2 fluxes in the Patagonia Sea: their relationship with fronts and chlorophyll distribution, J. Geophys. Res., 114, C03018, doi:10.1029/2008JC004854, 2009. 11737

Bovensmann, H., Burrows, J. P., Buchwitz, M., Frerick, J., Noel, S., Rozanov, V. V., Chance, K. V., and Goede, A. P. H.: SCIAMACHY – mission objectives and measurement modes, J. Atmos. Sci., 56(2), 127–150, 1999. 11732

Bracher, A., Vountas, M., Dinter, T., Burrows, J. P., Rttgers, R., and Peeken, I.: Quantitative observation of cyanobacteria and diatoms from space using PhytoDOAS on SCIAMACHY data, Biogeosciences, 6, 751–764, doi:10.5194/bg-6-751-2009, 2009. 11729, 11732

Brandini, F. P., Boltovskoy, D., Piola, A., Kocmur, S., Rottgers, R., Abreu, P. C., and Lopes, R. M.:

BGD
8, 11725–11765, 2011

Multiannual trends in fronts and distribution of nutrients and chlorophyll in the Southwestern Atlantic (30–62 S), Deep-Sea Res. Pt. I, 47, 1015–1033, 2000. 11737
Broecker, W. S. and Peng, T. H.: Tracers in the Sea, Eldigio, Palisades, New York, 1982. 11727
Brown, C. W.: Global Distribution of coccolithophore blooms, Oceanography, 8(2), 59–60, 1995. 11728, 11731
Brown, C. W. and Yoder, J. A.: Coccolithophorid blooms in the global ocean, J. Geophys. Res., 99(C4), 7467–7482, 1994a. 11728, 11729, 11731
Brown, C. W. and Yoder, J. A.: Distribution pattern of coccolithophorid blooms in the Western North Atlantic, Cont. Shelf Res., 14, 175–197, 1994b. 11728
Brown, C. W. and Podesta, G. P.: Remote sensing of coccolithophore blooms in the Western South Atlantic Ocean, Remote Sens. Environ., 60, 83–91, 1997. 11727, 11728, 11731
Burns, D. A.: Phenotypes and dissolution morphotypes of the genus *Gephyrocapsa Kamptner* and *Emiliania huxleyi* (Lohmann), N. Z. J. Geol. Geophys., 20(1), 143–155, 1977. 11731, 11738
Cai, W., Shi, G., Cowan, T., Bi, D., and Ribbe, J.: The response of the southern annular mode, the East Australian current, and the southern mid-latitude ocean circulation to global warming, Geophys. Res. Lett., 32, L23706, 2005. 11738
Carder, K. L., Chen, F. R., Cannizzaro, J. W., Campbell, J. W., and Mitchell, B. G.: Performance of the MODIS semi-analytical ocean color algorithm for chlorophyll-*a*, Adv. Space Res., 33, 1152–1159, 2004. 11728
Charlson, R. J., Lovelock, J. E., Andreae, M. O., and Warren, S. G.: Oceanic phytoplankton, atmospheric sulfur, cloud albedo and climate, Nature, 326, 655–661, doi:10.1038/326655a0, 1987. 11727, 11728
Clark, D. R., Flynn, K. J., and Owens, N. J. P.: The large capacity for dark nitrate-assimilation in diatoms may overcome nitrate limitation of growth, New Phytol., 155, 101–108, 2002. 11741
Erickson, D. J., Hernandez, J. L., Ginoux, P., Gregg, W. W., McClain, C., and Christian, J.: Atmospheric iron delivery and surface ocean biological activity in the Southern Ocean and Patagonian region, Geophys. Res. Lett., 30(12), 1609, doi:10.1029/2003GL017241, 2003. 11737
Falkowski, P. G., Barber, R. T., and Smetacek, V.: Biogeochemical controls and feedbacks on ocean primary production, Science, 281, 200–206, 1998. 11728
Garcia, C. A. E., Garcia, V. M. T., Dogliotti, A. I., Ferreira, A., Romero, S. I., Mannino, A., Souza, M. S., and Mata, M. M.: Environmental conditions and biooptical signa-

BGD
8, 11725–11765, 2011

ture of a coccolithophorid bloom in the Patagonian shelf, J. Geophys. Res., 116, C03025, doi:10.1029/2010JC006595, 2011. 11731, 11739
Goldman, J. C.: Potential role of large oceanic diatoms in new primary production, Deep-Sea Res. Pt. I, 40, 159–168, 1993. 11741
Goldman, J. C. and McGillicuddy, D. J.: Effect of large marine diatoms growing at low light on episodic new production, Limnol. Oceanogr., 48(3), 1176–1182, 2003.
Gordon, A. L.: Brazil Malvinas confluence-1984. Deep-Sea Res., 36(3), 359–384, 1989. 11736
Gordon, H. R. and Morel, A.: Remote Assessment of Ocean Color for Interpretation of Satellite Visible Imagery: a Review, Springer-Verlag, New York, 1983. 11730
Gordon, H. R., Brown, O. B., Evans, R. H., Brown, J. W., Smith, R. C., Baker, K. S., and Clark, D. K.: A semi-analytic radiance model of ocean color, Geophys. Res., 93, 10909–10924, 1988. 11730, 11739
Gordon, H. R., Boynton, G. C., Balch, W. M., Groom, S. B., Harbour, D. S., and Smyth, T. J.: Retrieval of coccolithophore from SeaWiFS imagery calcite concentration, Geophys. Res. Lett., 28(8), 1587–1590, 2001. 11728, 11729
Gregg, W. W., and Casey, N. W.: Modeling coccolithophores in the global oceans, Deep-Sea Res. Pt. II, 54(5–7), 447–477, 2007. 11729
Gregg, W. W., Ginoux, P., Schopf, P. S., and Casey, N. W.: Phytoplankton and iron: validation of a global three-dimensional ocean biogeochemical model, Deep-Sea Res. Pt. II, 50, 3147–3169, 2003. 11729
Groom, S. and Holligan, P. M.: Remote sensing of coccolithophore blooms, Adv. Space Res., 7 (2), 73–78, doi:10.1016/0273-1177(87)90166-9, 1987. 11728
Holligan, P. M., Viollier, M., Harbour, D. S., and Champagne-Philipe, M.: Satellite and ship studies of coccolithophore production along a continental shelf-edge, Nature, 304, 339–342, 1983. 11727, 11728, 11736
Holligan, P. M., Fernandez, E., Aiken, J., Balch, W. M., Boyd, P., Burkill, P. H., Finch, M., Groom, S. B., Malin, G., Muller, K., Purdie, D. A., Robinson, C., Trees, C. C., Turner, S. M., and Van der Wal, P.: A biogeochemical study of the coccolithophore Emiliania huxleyi in the north Atlantic, Global Biogeochem. Cy., 7(4), 879–900, 1993. 11728, 11731, 11739
Keller, M. D., Bellows, W. K., and Guillard, R. R. L.: Dimethylsulfide production and marine phytoplankton: an additional impact of unusual blooms, in: Novel Phytoplankton Blooms, edited by: Cosper, E. M., Bricelj, V. M., and Carpenter, E. J., Springer-Verlag, New York, 101–115, 1989b. 11728

BGD
8, 11725–11765, 2011

Lochte, K., Ducklow, H. W., Fasham, M. J. R., and Stienen, C.: Plankton succession and carbon cycling at 47-degrees-N–20-degrees-W during the JGOFS North Atlantic bloom experiment, Deep-Sea Res. Pt. II, 40(1–2), 91–114, 1993. 11728

Longhurst, A. R.: Seasonal cycles of pelagic production and consumption, Progr. Oceanogr., 36, 77–167, 1995. 11737

Longhurst, A. R.: Ecological Geography of the Sea, Academic Press, San Diego, 1998, ISBN: 0-12-455559-4. 11745

Malin, G., Turner, S. M., and Liss, P. S.: Sulfur: the plankton/climate connection, J. Phycol., 28(5), 590–597, 1992. 11728

Margalef, R.: Life-forms of phytoplankton as survival alternatives in an unstable environment, Oceanol. Acta, 1, 493–509, 1978. 11728, 11736

Milliman, J. D.: Production and accumulation of calcium in the ocean, Global Biogeochem. Cy., 7, 927–957, 1993. 11727

Morozov, E., Korosov, A., Pozdnyakov, D., Pettersson, L., and Sychev, V.: A new area-specific bio-optical algorithm for the Bay of Biscay and assessment of its potential for SeaWiFS and MODIS/Aqua data merging, Int. J. Remote Sens., 31(24), 6541–6565, 2010. 11728

Nair, A., Sathyendranath, S., Platt, T., Morales, J., Stuart, V., Forget, M.-H., Devred, E., and Bouman, H.: Remote sensing of phytoplankton functional types, Remote Sens. Environ., 112, 3366–3375, 2008. 11729

Nanninga, H. J. and Tyrrell, T.: Importance of light for the formation of algal blooms by Emiliania huxleyi, Mar. Ecol.-Prog. Ser., 136, 195–203, 1996. 11740, 11745

Neuheimer, A. B., Thresher, R. E., Lyle, J. M., and Semmens, J. M.: Tolerance limit for fish growth exceeded by warming waters, Nature Climate Change, 1, 110–113, doi:10.1038/nclimate1084, 2011. 11737

Oliveira, L. R., Piola, A. R., Mata, M. M., and Soares, I. D.: Brazil Current surface circulation and energetics observed from drifting buoys, J. Geophys. Res., 114, C10006, doi:10.1029/2008JC004900, 2009. 11737

O'Reilly, J. E., Maritorena, S., Mitchell, B. G., Siegel, D. A., Carder, K. L., Garver, S. A., Kahru, M., and McClain, C.: Ocean color chlorophyll algorithms for SeaWiFS, J. Geophys. Res., 103(C11), 24937–24953, 1998. 11728

Painter, S. C., Poulton, A. J., Allen, J. T., Pidcock, R., and Balch, W. M.: The COPAS'08 expedition to the Patagonian Shelf: physical and environmental conditions during the 2008 coccolithophore bloom, Cont. Shelf Res., 30, 1907–1923, 2010. 11731, 11737, 11739

BGD
8, 11725–11765, 2011

Perner, D. and Platt, U.: Detection of nitrous acid in the atmosphere by differential optical absorption, Geophys. Res. Lett., 93, 917–920, 1979. 11729

Platt, U.: Differential optical absorption spectroscopy (DOAS), in: Air Monitoring by Spectroscopic Techniques, edited by: Sigrist, M., John Wiley & Sons, Inc., 27–84, 1994. 11729

Raitsos, D. E., Lavender, S. J., Pradhan, Y., Tyrrell, T., Reid, P. C., and Edwards, M.: Coccolithophore bloom size variation in response to the regional environment of the subarctic North Atlantic, Limnol. Oceanogr., 51, 2122–2130, 2006. 11731, 11735, 11736, 11739, 11740, 11745

Raven, J. A. and Falkowski, P. G.: Oceanic sinks for atmospheric CO_2, Plant Cell Environ., 22, 741–755, 1999. 11727

Rhodes, L. L., Peake, B. M., MacKenzie, A. L., and Marwick, S.: *Coccolithophores Gephyrocapsa oceanica* and *Emiliania huxleyi* (Prymnesiophyceae = Haptophyceae) in New Zealand's coastal waters: characteristics of blooms and growth in laboratory culture, New Zeal. J. Mar. Freshw. Res., 29(3), 345–357, 1995. 11738

Ridgway, K. R.: Long-term trend and decadal variability of the southwardpenetration of the East Australian current, Geophys. Res. Lett., 34, L13613, 2007. 11738

Riebesell, U., Zondervan, I., Rost, B., Tortell, P. D., Zeebe, R. E., Morel, F. M. M.: Reduced calcification of marine plankton in response to increased atmospheric CO_2, Nature, 407, 364–367, doi:doi:10.1038/35030078, 2000. 11727

Romero, S. I., Piola, A. R., Charo, M., and Garcia, C. A. E.: Chlorophyll-*a* variability off Patagonia based on SeaWiFS data, J. Geophys. Res., 111, C05021, doi:10.1029/2005JC003244, 2006. 11737

Rost, B. and Riebesell, U.: Coccolithophores and the biological pump: Responses to environmental changes, in: Coccolithophores, from Molecular Processes to Global Impact, edited by: Thierstein, H. R. and Young, J. R., 99–126, Springer, New York, 2004. 11727, 11728

Sabatini, M. E., Reta, R., and Matano, R.: Circulation and zooplankton biomass distribution over the Southern Patagonian shelf during late summer, Cont. Shelf Res., 24, 1359–1373, doi:10.1016/j.csr.2004.03.014, 2004. 11737

Sadeghi A., Dinter T., Vountas M., Taylor B., and Bracher, A.: Improvements to PhytoDOAS method for identification of major phytoplankton groups using hyper-spectral data, Ocean Sci. Discuss., 8, 2271-2311, doi:10.5194/osd-8-2271-2011, 2011. 11729, 11731, 11732

Saraceno, M., Provost, C., Piola, A. R., Bava, J., and Gagliardini, A.: Brazil Malvinas Frontal System as seen from 9 years of advanced very high resolution radiometer data, J. Geophys.

BGD
8, 11725–11765, 2011

Res., 109, C05027, doi:10.1029/2003JC002127, 2004. 11737
Sathyendranath, S., Watts, L., Devred, E., Devred, E., Platt, T., Caverhill, C., and Maass, H.: Discrimination of diatoms from other phytoplankton using ocean-colour data, Mar. Ecol.-Prog. Ser., 272, 59–68, 2004. 11728, 11729
Schloss, I. R., Ferreyra, G. A., Ferrario, M. E., Almandoz, G. O., Codna, R., Bianchi, A. A., Balestrini, C. F., Ochoa, H. A., Pino, D. R., and Poisson, A.: Role of plankton communities in sea-air variations in pCO_2 in the SW Atlantic Ocean, Mar. Ecol.-Prog. Ser., 332, 93–106, 2007. 11737
Smyth, T. J., Tyrrell, T., and Tarrant, B.: Time series of coccolithophore activity in the Barents Sea, from twenty years of satellite imagery, Geophys. Res. Lett., 31, L11302, doi:10.1029/2004GL019735, 2004. 11728
Spadone, A. and Provost, C.: Variations in the Malvinas Current volume transport since October 1992, J. Geophys. Res., 114, C02002, doi:10.1029/2008JC004882, 2009. 11736
Subramaniam, A., Brown, C. W., Hood, R. R., Carpenter, E. J., and Capone, D. G.: Detecting *Trichodesmium* blooms in SeaWiFS imagery, Deep-Sea Res. Pt. II, 49, 107–121, 2002. 11729
Thierstein, H. R. and Young, J. R.: Coccolithophores from Molecular Processes to Global Impact, Springer, New York, 2004. 11728
Tilburg, C. E., Subrahmanyam, B., and O'Brien, J. J.: Ocean color variability in the Tasman Sea, Geophys. Res. Lett., 29(10), 1487–1481, doi:10.1029/2001GL014071, 2002. 11731, 11738, 11740, 11742, 11743
Tyrrell, T. and Taylor, A. H.: A modelling study of *Emiliania huxleyi* in the NE Atlantic, J. Mar. Syst., 9, 83–112, 1996. 11740
Tyrrell, T. and Merico, A.: *Emiliania huxleyi*: Bloom Observations and the Conditions that Induce Them, in: Coccolithophores from Molecular Processes to Global Impact, edited by: Thierstein, H. R. and Young, J. R., Springer, New York, 75–97, 2004. 11727
Tyrrell, T., Holligan, P. M., and Mobley, C. D.: Optical impacts of oceanic coccolithophore blooms, J. Geophys. Res., 104(C2), 3223–3241, 1999. 11727, 11729
Van der Linden, W. J. M.: Extinct mid-ocean ridges in the Tasman sea and in the Western Pacific, Earth Planet. Sci. Lett., 6, 483–490, 1969. 11740
Vountas, M., Richter, A., Wittrock, F., and Burrows, J. P.: Inelastic scattering in ocean water and its impact on trace gas retrievals from satellite data, Atmos. Chem. Phys., 3, 1365–1375, doi:10.5194/acp-3-1365-2003, 2003. 11732

BGD
8, 11725–11765, 2011

Vountas, M., Dinter, T., Bracher, A., Burrows, J. P., and Sierk, B.: Spectral studies of ocean water with space-borne sensor SCIAMACHY using Differential Optical Absorption Spectroscopy (DOAS), Ocean Sci., 3, 429–440, doi:10.5194/os-3-429-2007, 2007. 11733

Westbroek, P., De Vring-De Jong, E. W., Van Der Wal, P., Borman, A. H., and De Vring, J. P. M.: Biopolymer-mediated Ca and Mn accumulation and biomineralization, Geol. Mijnbouw, 64, 5–15, 1985. 11727

Westbroek, P., Brown, C. W., Van-Bleijswijket, J., Brownlee, C., Brummer, G.J., Conte, M., Egge, J., Fernandez, E., Jordan, R. W., Knappertsbusch, M., Stefels, J., Veldhuis, M., Vander-Wal, P., and Young, J. R.: A model approach to biological climate forcing. The example of Emiliania huxleyi, Global Planet. Change, 8, 27–46, 1993. 11728

Winder, M. and Cloernet, J. E.: The annual cycles of phytoplankton biomass, Phil. T. R. Soc., 365, 3215–3226, 2010. 11730

Yoder, J. A., McClain, C. R., Feldman, G. C., and Esaias, W. E.: Annual cycles of phytoplankton chlorophyll concentrations in the global ocean: a satellite view, Global Biogeochem. Cy., 7(1), 181–193, 1993. 11728

BGD
8, 11725–11765, 2011

Table 1. MLD trends in selected regions.

Region	Simple trend	Anomaly trend
nAtl	–0.660	0.050
sAtl	–0.219	–0.271
sPac	–0.081	–0.232

BGD
8, 11725–11765, 2011

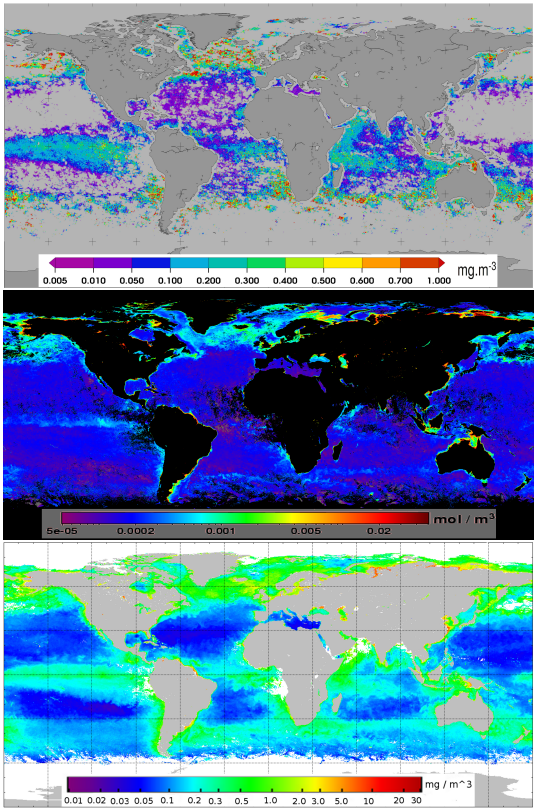

Fig. 1. A sample comparison of three monthly mean products, all obtained in August 2005: the PhytoDOAS *coccos* chl-*a* (upper panel) retrieved from SCIAMACHY data, the PIC concentration (middle panel) from the MODIS-Aqua level-3 products, and the total chl-*a* (lower panel) from the GlobColour level-3 merged data.

BGD
8, 11725–11765, 2011

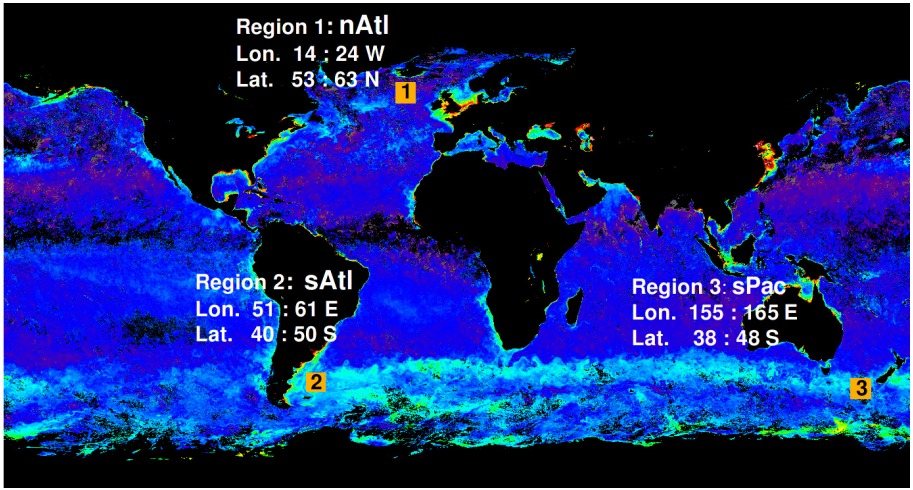

Fig. 2. Selected regions for monitoring the development of *coccos* blooms in this study. Each region has the geographical size of $10^{\circ} \times 10^{\circ}$; regions 1, 2 and 3 have been named as *nAtl*, *sAtl* and *sPac*, respectively. The background image shows the PIC monthly-mean conc. in March 2005 from the MODIS-Aqua level-3 products, demonstrating the *Great Calcite Belt* as a bright greenish band above the sub-Antarctic regions.

BGD
8, 11725–11765, 2011

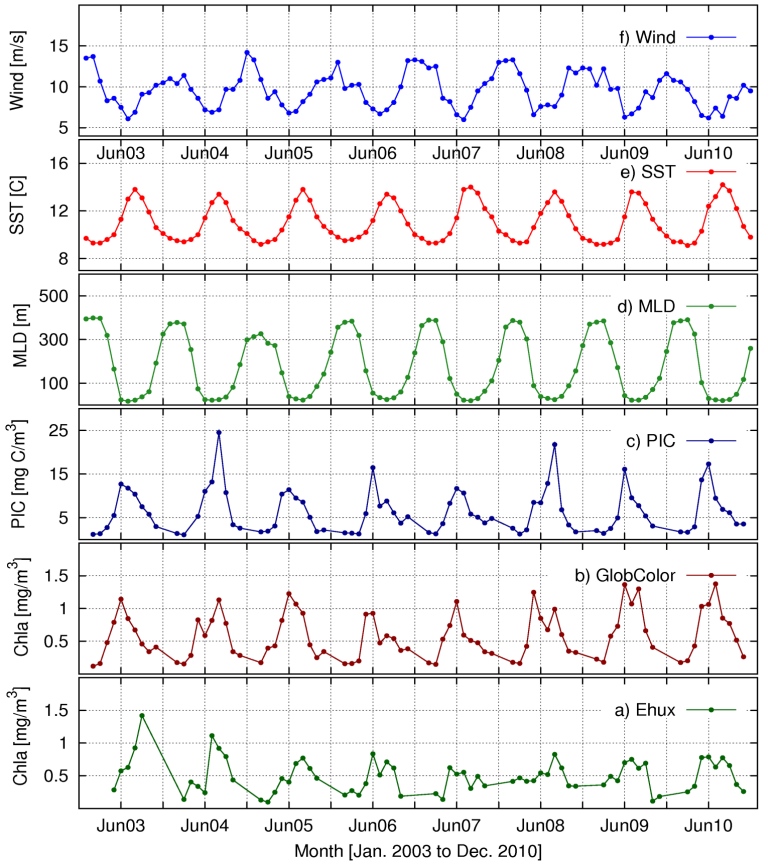

Fig. 3. Time series of six parameters monitored in *nAtl* from January 2003 to December 2010: **(a)** *coccos* [*Ehux*] chl-*a* conc. retrieved by PhytoDOAS; **(b)** GlobColour total chl-*a*; **(c)** MODIS-Aqua PIC conc.; **(d)** MLD from Ocean Productivity; **(e)** SST from AVHRR; and **(f)** surface wind-speed from AMSR-E.

BGD
8, 11725–11765, 2011

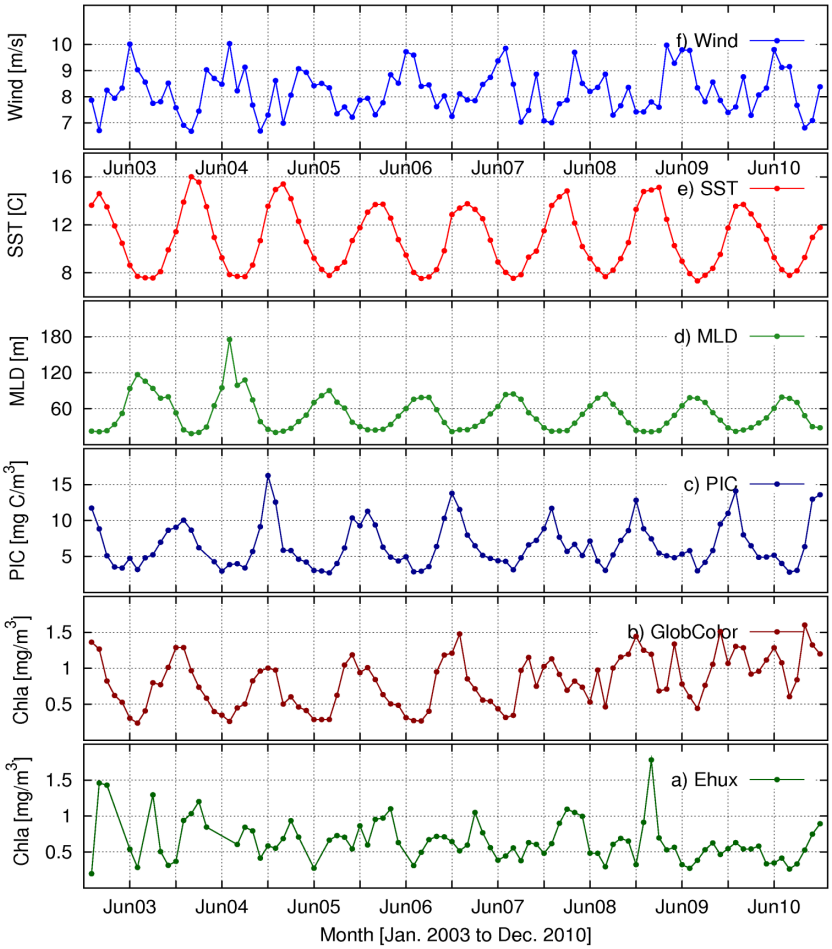

Fig. 4. Time series as described in Fig. 3, but for the *sAtl* region.

BGD
8, 11725–11765, 2011

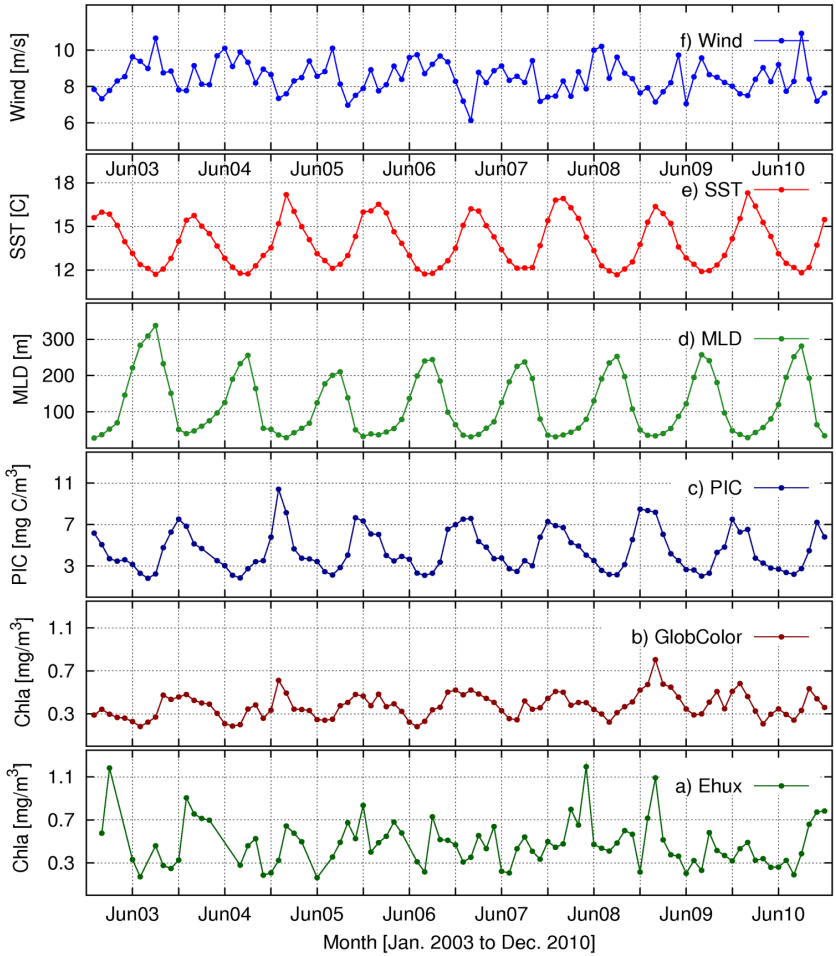

Fig. 5. Time series as described in Fig. 3, but for the *sPac* region.

BGD
8, 11725–11765, 2011

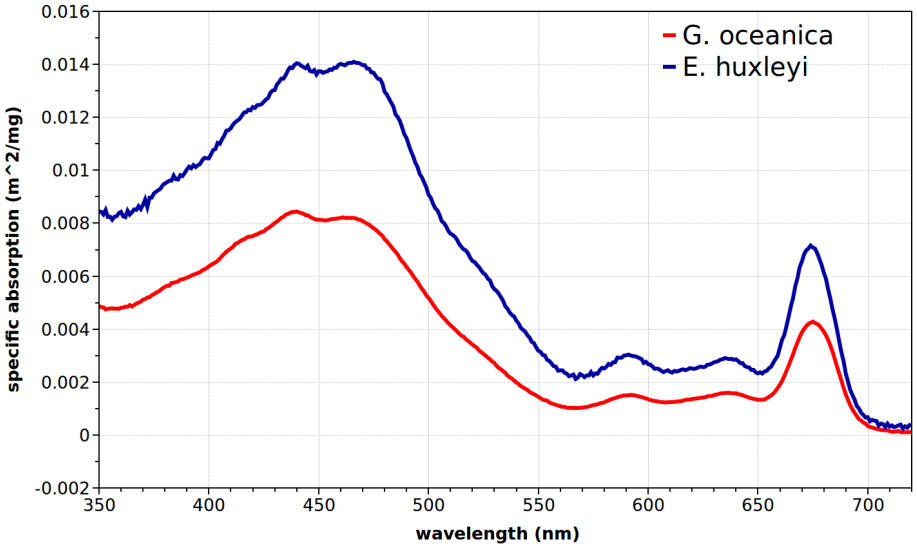

Fig. 6. Specific absorption spectra of two different *coccos* species obtained from cultures: *G. oceanica* (red), isolated from the North Atlantic near the Portuguese coast; and *E. huxleyi*, isolated from the Tasman Sea in the South-West Pacific.

BGD
8, 11725–11765, 2011

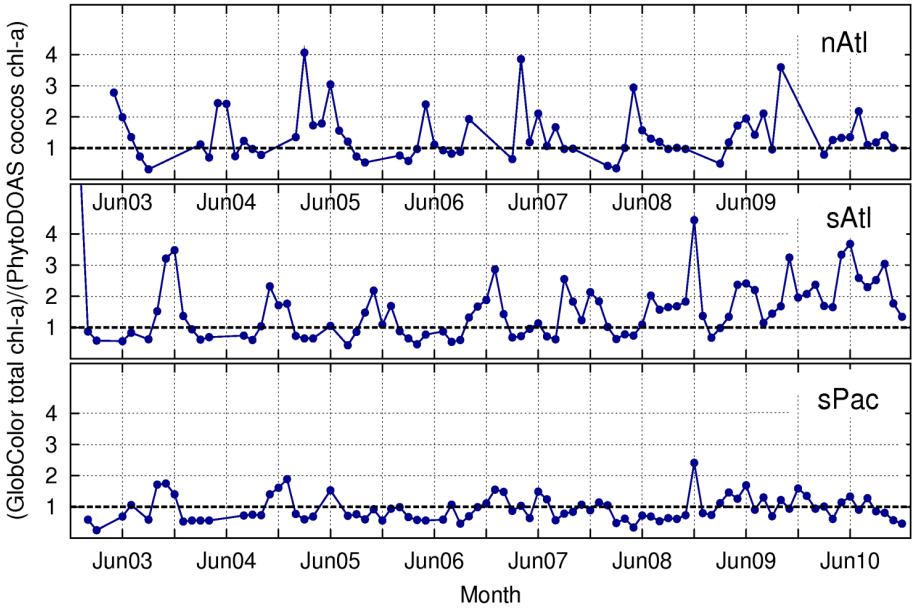

Fig. 7. Ratios of the GlobColour total chl-*a* to the PhytoDOAS retrieved chl-*a* of *coccos* in three selected regions: *nAtl* (upper panel), *sAtl* (middle panel) and *sPac* (lower panel).

BGD
8, 11725–11765, 2011

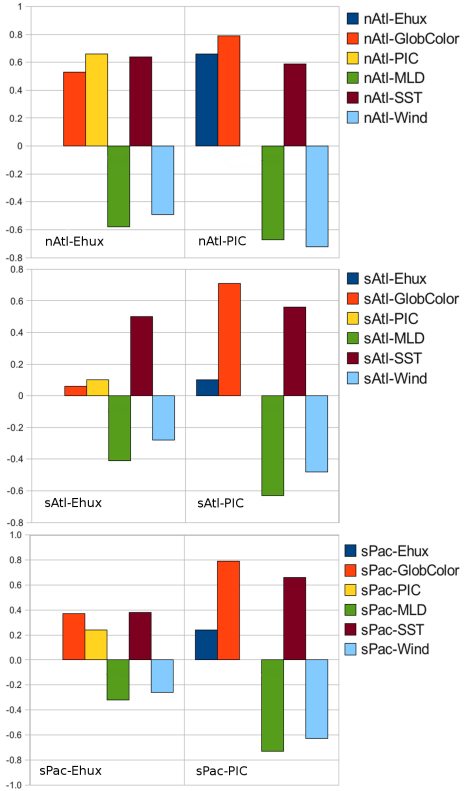

Fig. 8. Correlation coefficients between the time series of PhytoDOAS *coccos* [*Ehux*] chl-*a* (left panels) and the other parameters in the three investigated regions: *nAtl* (upper panel), *sAtl* (middle panel) and *sPac* (lower panel). The same quantity is depicted on the left panels between the time series of PIC and the other parameters for three regions, respectively.

BGD
8, 11725–11765, 2011

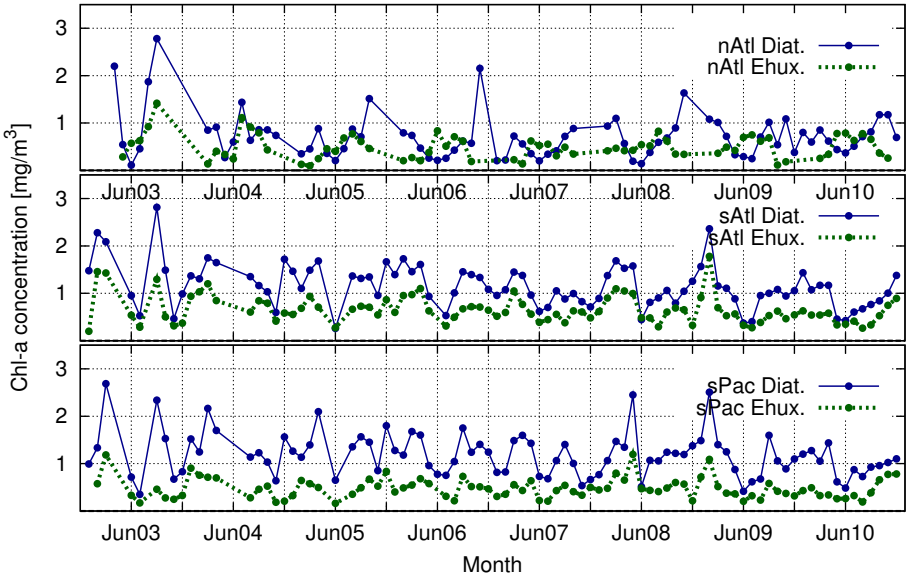

Fig. 9. Times series of the PhytoDOAS diatoms (blue solid lines) and *coccos* (green dashed lines) chl-*a* in the three selected regions: *nAtl* (lower panel), *sAtl* (middle panel) and *sPac* (upper panel).

BGD
8, 11725–11765, 2011

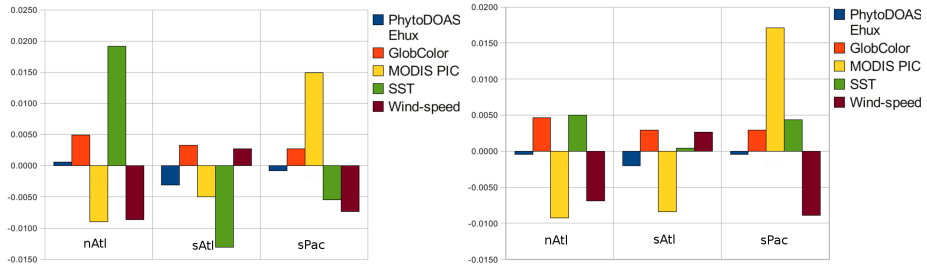

Fig. 10. Linear trends of five monitored parameters over eight years data (2003 to 2010) in three selected regions: *nAtl* (left), *sAtl* (middle) and *sPac* (right). The left panels show the values of the *simple trends*, while the right panels show the values of the *anomaly trends*. In both cases only the regional spring and summer months were considered, which means: April to September for *nAtl* and September to March for *sAtl* and *sPac*. The chart does not include the MLD trends, due to their different ranges, being much higher in order of magnitude.

BGD
8, 11725–11765, 2011

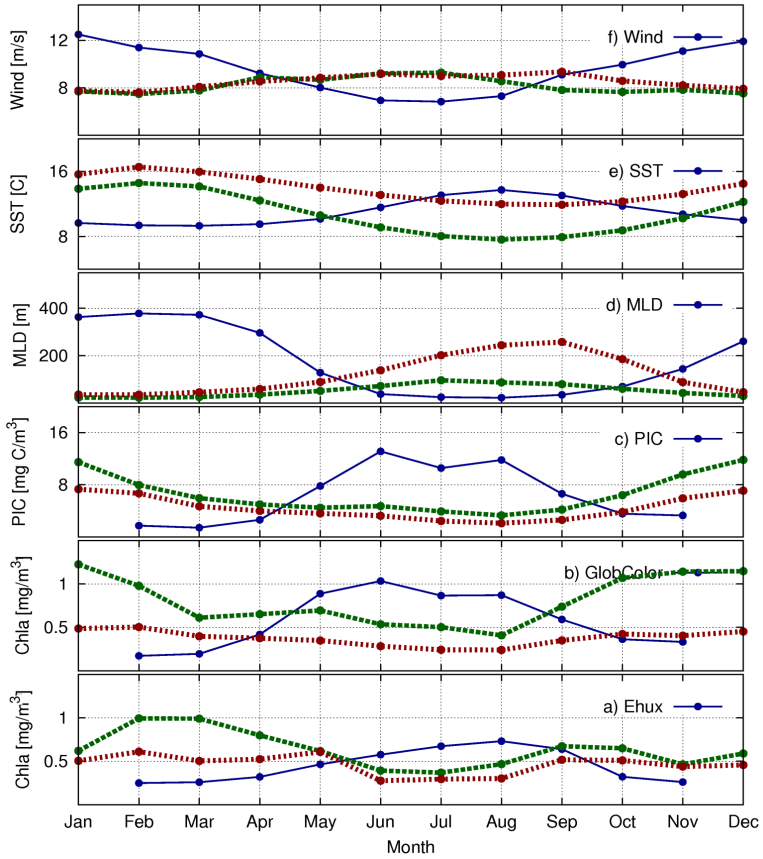

Fig. 11. Climatology curves of all monitored parameters in three selected regions. Each subplot contains the climatologies of a certain parameter in three regions, which are denoted as follows: *nAtl* (blue line), *sAtl* (green dashed-line) and *sPac* (red dashed-line). The subplots have been arranged in the same order as before: **(a)** *coccos* chl-*a* conc.; **(b)** GlobColour total chl-*a*; **(c)** PIC conc.; **(d)** MLD **(e)** SST, and **(f)** surface wind-speed.

BGD
8, 11725–11765, 2011